Weld Ductility Studies of a Tin-Modified Copper-Nickel Alloy

Manganese and phosphorus additions eliminated cracking that resulted from gamma formation at grain boundaries

BY M. TUMULURU AND E. F. NIPPES

ABSTRACT. The ductility of gas tungsten arc (GTA) and plasma transferred arc (PTA) welds made on Cu-9 Ni-6 Sn alloy was studied using a three-point, slow-bend test. The variables studied included the addition of manganese, phosphorus and zinc to the alloy, and the effect of shielding gases. A few welds were prepared in an environmental chamber containing argon to eliminate the possibility of atmospheric contamination of the weld pool. Gleeble simulations in an argon atmosphere were conducted on some of the heats to study the mechanism of crack formation in the welds. In addition, scanning electron microscope (SEM) and optical metallographic techniques were utilized to study selected welds and Gleeble specimens to characterize the crack morphology and porosity levels. Oxygen, nitrogen and hydrogen contents of the alloy were determined for the as-cast condition, the homogenized condition and for welded specimens.

The results indicated that the cause of weld failures in the bend test was the initiation of cracks from the tin-rich Gamma phase that formed along the grain boundaries in the partially melted zone. The addition of manganese and phosphorus to the alloy together with the use of argon-5% hydrogen shielding gas mixture in plasma arc welding produced ductile welds with reduced levels of porosity.

KEY WORDS

Weld Ductility
Partially Melted Zone
Tin-Modified Cu-Ni
Mn-P Additive Effect
HAZ Cracking
Bend Test Failures
Porosity
Sn-Rich Gamma Cracks
GTA Welding
Plasma Arc Welding

M. TUMULURU is a Research Assistant, Dept. of Welding Engineering, Ohio State University, Columbus, Ohio. E. F. NIPPES is Professor Emeritus, Dept. of Materials Engineering, Rensselaer Polytechnic Institute, Troy, N.Y.

Introduction

High spring strength, good formability coupled with high electrical conductivity and corrosion resistance make tin-modified copper-nickel alloys attractive for use in electronic connector applications. Typical applications of these alloys include items such as connectors, diaphragm members, spring components in electromechanical packages and ocean cable hardware (Refs. 1, 2). Alloys such as Cu-9Ni-6Sn and Cu-4Ni-8Sn (nominal compositions) are typically made by thin-section, continuous-slab casting because the solidification rates in this process minimize segregation of tin (Ref. 3). Otherwise, segregation of tin during solidification can lead to hot shortness and difficulties in homogenizing the cast structure.

The room-temperature microstructure of Cu-9Ni-6Sn as-cast alloy shows the presence of a tin-rich phase Gamma (γ) in the interdendritic regions. As can be seen from the phase diagram of Cu-9 Ni and Sn (Fig. 1), the tin-rich Gamma is an intermetallic compound of the type (Cu, Ni)$_3$ Sn. The fact that the Gamma phase forms in the interdendritic regions suggests that it is the last-to-solidify constituent during the solidification of this alloy. Intermetallic compounds such as (Cu, Ni)$_3$ Sn are brittle and often suffer crack initiation under stress. Therefore, the presence of Gamma phase in or near the weld can cause welds in Cu-9 Ni-6 Sn alloy to crack due to the initiation of microcracks at Gamma phase regions.

The continuously cast slabs in the Cu-Ni-Sn alloys are rolled to thinner gauges, which are heat treated to improve their ductility and welded to produce long coils. These long coils are then further cold rolled to final gauges. Because the welds see considerable amounts of bending during the coiling and uncoiling operations, it is important that the welds possess adequate bend ductility and strength to withstand a wide variety of stresses that they are subjected to during these operations. Many mechanical properties, such as fatigue strength and yield strength, of these copper-nickel-tin alloys have been studied by earlier researchers (Refs. 4, 5). However, no literature is available on the

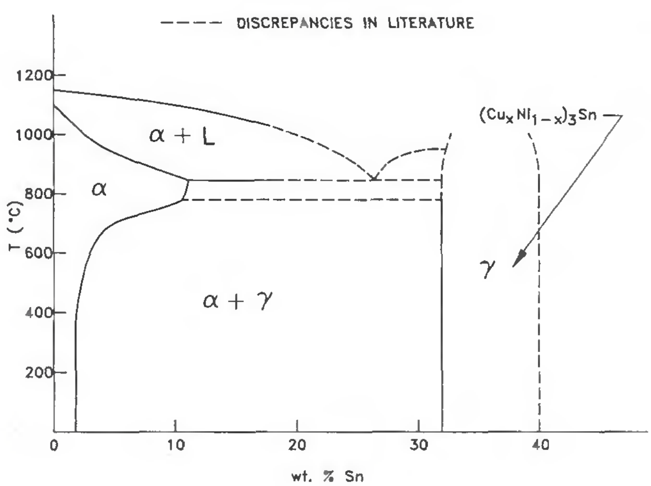

Fig. 1 — Pseudo binary phase diagram of (Cu-9 Ni)-Sn.

Table 1—Alloying Additions to the Melts

Heat No.	Mn	P	Zn	Alloy Type (nominal composition)
1	none	none	none	Cu-9 Ni-6 Sn
2	0.1	0.01	none	Cu-9 Ni-6 Sn
3	0.1	0.01	0.20	Cu-9 Ni-6 Sn
4	0.1	0.01	none	Cu-9 Ni

weldability of these alloys.

Porosity in the weldments is a major problem faced during the autogenous welding of copper and its alloys (Refs. 6–9). It has been reported that the number and size of pores in the weld metal in copper alloys depend on the rate of cooling of the weld metal and the nature of the gas evolved during the solidification of the weld (Ref. 7). If hydrogen and oxygen are present in the base metal, porosity can still occur in the weld even if neither gas is supplied through external sources such as shielding gas or atmosphere surrounding the arc (Ref. 7). Porosity forms in the weld as a result of the evolution of either hydrogen or water vapor.

Although oxygen alone is not considered to cause any porosity in the weld metal, it may cause problems when cuprous oxide reacts with atomic hydrogen in the molten metal to form water vapor and result in the formation of large pores (Refs. 10, 11). These large pores, in turn, result in loss in cross-sectional area and proportionally lower tensile strength of the weld. Embrittlement of the heat-affected zone can also result due to the formation of cuprous oxide during solidification (Refs. 7, 12). Therefore, copper and its alloys should be effectively deoxidized and contain no hydrogen in order to eliminate completely the possibility of porosity formation in the welds (Ref. 13). Furthermore, the elimination of hydrogen is especially important because even as little as 1 ppm H results in a gas evolution equivalent to 44% of the volume of the metal (Ref. 8).

Nazerenko, *et al.*, found that the roughness of the butt edges and the contamination of the faying surfaces played a significant role in the formation of porosity in welds (Ref. 14). They also found that more porosity formed in welds on butt joints than in beads-on-plate. Studying the porosity formation in aluminum weld metal, Uda and Ohno found that the size and the extent of pores increased with increasing hydrogen partial pressure and temperature (Ref. 15). Uda and Ohno further observed that the gas bubbles were not formed in the solid-liquid interface but were already formed in the liquid metal under rapid cooling conditions.

Although several researchers pointed to the occurrence of steam porosity in copper-alloy welds (Refs. 7–9, 16), Littleton and Jordon were the first to confirm experimentally that porosity can result in gas tungsten arc (GTA) welding of copper by the occurrence of steam reaction in the weld pool (Ref. 17). They explained the occurrence of steam porosity in the weld metal using a weld-pool model proposed by Howden and Milner (Ref. 18).

Many investigators found that nitrogen can also cause porosity in the gas shielded welding of copper (Refs. 19–24). This problem from nitrogen was found to be more acute in gas tungsten arc welding than in gas metal arc (GMA) welding (Ref. 19). The porosity from nitrogen can be reduced by the use of increased welding speed and the use of denitriding elements such as titanium in the filler metal (Refs. 19–23). Using helium as shielding gas and multipass gas tungsten arc welding technique, Brandon was able to produce porosity-free welds in boron-deoxidized copper (Ref. 26).

The object of this investigation was to study the ductility behavior of the autogenous gas tungsten arc and plasma transferred arc (PTA) welds made on copper-9 nickel-6 tin (nominal composition) alloy using slow bend tests. In addition, the object included studying, using Gleeble simulations, the effect of various alloying additions, such as Zn, Mn and P, on the ductility of the welds in the copper-9 nickel-6 tin alloy.

Materials and Experimental Procedure

The tin-modified copper-nickel alloy used in this study is designated by UNS No. C72700. Its chemical composition is covered under ASTM standard B740-87 (Ref. 27). All materials used in the study were continuously cast in 34-kg (75-lb.) slabs from high-purity, virgin charges. The alloying additions made to the various heats cast are listed in Table 1. The cast slabs were 12.5 mm (0.5 in.) thick by 87.5 mm (3.5 in.) wide. The 75-mm (3-in.) long sections cut from the as-cast slabs were cold rolled to 5 mm (0.2 in.), homogenized at 900°C (1650°F) under nitrogen atmosphere and cooled in a stream of air from a fan. The strips were wire brushed prior to welding to remove the scale. The faces to be welded were sheared to have a good contact.

Autogenous gas tungsten arc and plasma transferred arc (PTA) welds were made transverse to the rolling direction of the strips. Table 2 lists the welding conditions used in the study. The welding conditions were chosen to give full-penetration welds. A few GTA welds were also made on Heat No. 2 in an environmental chamber to diminish any atmospheric contamination of the weld pool. A schematic of the environmental chamber is shown in Fig. 2. After the pieces to be welded were placed in the chamber and the chamber sealed, it was purged with argon at 18.9 L/min (40 cfh) for 15 minutes to drive air from the chamber. During welding, half of the argon flowed through the torch as shielding gas while the remainder flowed through the inlet into the chamber. The chamber was purged with argon for 10 minutes after each weld was completed. Indeed, prior to welding, the argon-purged chamber contained less than 60 ppm oxygen.

Plasma arc welding was done in air using argon as the orifice gas and argon - 5% hydrogen as the shielding gas. A shielding gas of argon with a flow rate of 4.7 L/min was used on the bottom side of the weld. This gas flowed through holes drilled in the back-up chill bar to minimize oxidation of the root of the weld. Some plasma arc welds were also made using argon as the shielding gas. All plasma arc welds in the study were made in key-hole mode (Ref. 28).

Strips 125 × 40 mm (5 × 1.6 in.) were cut transverse to the welds for bend testing. Both root and face bend tests were performed on all welds. Three-point, slow-bend testing was done on an Instron machine. A crosshead travel speed of 12.5 mm/min (0.5 in./min) was used for bending the welds. A drop in the load during the bend tests usually denoted the initiation of cracks. The bend angle the welds experienced before crack initiation was recorded in each case. The welds were bent up to a maximum of 130 deg.

Specimens measuring 150 × 25 × 2.5 mm (6 × 1 × 0.1 in.) were prepared by cold rolling the homogenized 5-mm (0.2-in.) thick strips for simulating the weld

Table 2—Welding Conditions Used in the Study

Gas Tungsten Arc Welding	
Current (A)	220–240
Travel speed (mm/min)	100
Voltage (V)	12.0
Shielding gas	Argon
Gas flow rate (L/min)	18.9
Electrode size and type	3.2 mm diameter 2% Thoriated tungsten
Plasma Arc Welding	
Current (A)	135–150
Travel Speed (mm/min)	225
Voltage	25
Shielding gas (L/min)	11.8
Back-up gas (argon) flow rate (L/min)	4.7
Plasma gas flow rate (L/min)	1.7
Electrode size and type	4.8 mm diameter 2% Thoriated tungsten
Electrode standoff distance (mm)	3.17

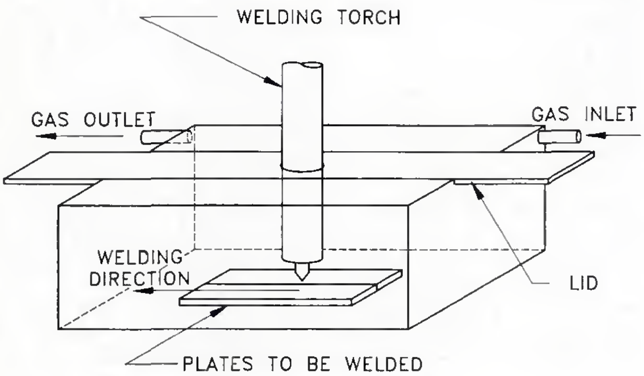

Fig. 2 — Environmental chamber for GTA welding.

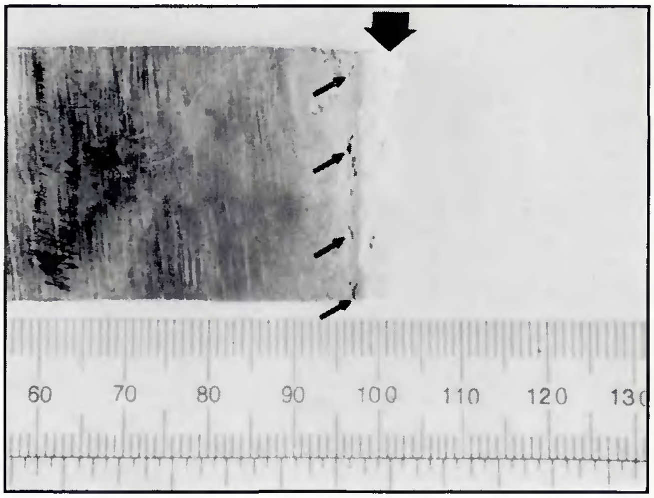

Fig. 3 — Location of cracks in a broken weld from Heat 1 (shown by small arrows). The large arrow shows the weld.

heat-affected zones in a Gleeble.

The Gleeble simulations were performed on Heats 1, 2 and 3 only. The specimens were heated in a Gleeble in an argon atmosphere from room temperature to 850°C (1562° F) at 50°C/s (90° F/s) and from 850°C to the peak temperature at 2.5°C/s (4.5° F/s). They were then held at the peak temperature for 10 seconds and were allowed to cool in argon. The peak temperatures selected for the study were 950° to 1050°C (1742° to 1922° F) at 25°C (45° F) increments. Two specimens were tested from each temperature group; one of these was subjected to bend testing.

Oxygen, nitrogen and hydrogen contents were measured in samples from Heat 1 in the as-cast condition in the as-homogenized condition and in the weld metal. The oxygen and nitrogen contents were measured using a LECO TC-136 gas analyzer. This instrument is capable of detecting both oxygen and nitrogen up to 0.1 ppm when using a gram weight sample. It can also accurately determine both the gases up to 1% of the gases present. Five specimens were tested in each case and averages calculated.

The hydrogen analyses were performed on a LECO HW-200 hydrogen determinator on duplicate samples. A 25-min, 600°C (1112° F) thermal cycle was utilized to liberate diffusible hydrogen from the samples. To assure that molecular hydrogen contained in pores would be liberated, analyses were carried out in the liquid state at 600°C in dehydrogenized crucibles containing dehydrogenized tin. Copper-tin alloys containing more than 67% tin are completely liquid at 600°C. The error in analysis for a 10-g sample at a hydrogen level of 0.5 ppm is estimated as ±0.05 ppm.

Selected welds and the remainder of the Gleeble specimens were sectioned, mounted, polished and studied under an optical microscope. Selected welds from the bend tests were also studied under a scanning electron microscope with an energy dispersive x-ray (EDX) fluorescence spectrometer.

Results

Bend Test Results

All welds from Heat No. 1 broke in the bend tests. Cracks initiated in the bend specimens even before the deformation in bending reached 30 deg. The weld failure in most cases occurred adjacent to the weld in the heat-affected zone — Fig. 3. However, cracks were also noticed in a few of the weld fusion zones. Some of the welds totally fell apart before the bend angle reached 60 deg.

The gas tungsten arc (GTA) welds made on Heat Nos. 2 and 3 showed improvement over those from Heat No. 1 in that they withstood more bending before cracks initiated in them. Although the GTA welds from Heat Nos. 2 and 3 did not totally fall apart in the bend tests, they showed deep weld cracks that would make them unsatisfactory for service performance. The porosity levels in GTA welds from Heats 2 and 3 were noticeably lower compared to those from Heat No.

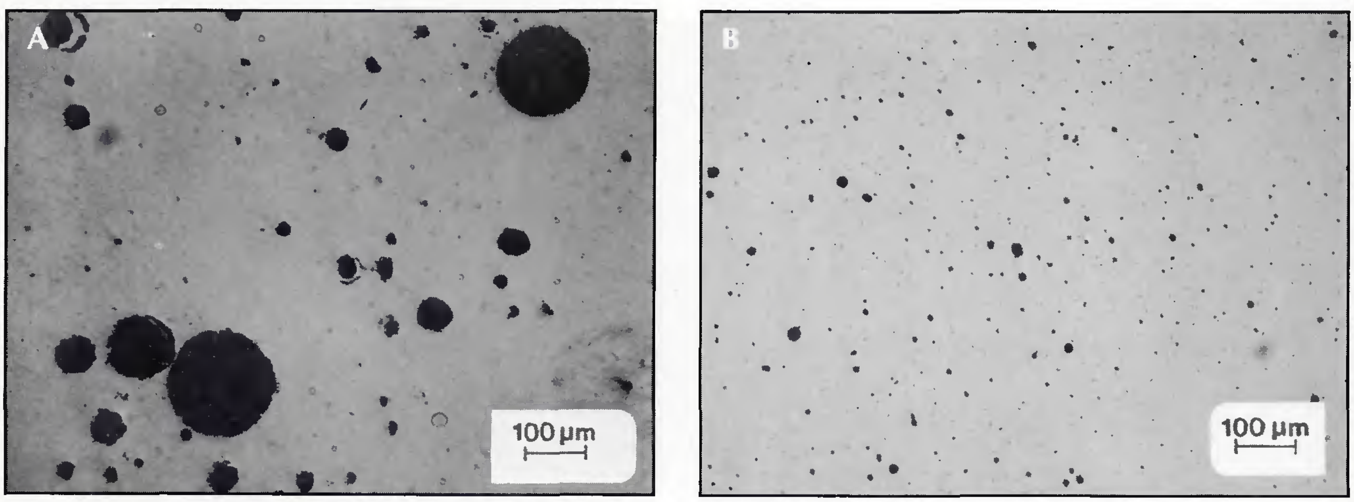

Fig. 4 — Porosity levels in GTA welds (as-polished). A — Heat 1; B — Heat 3.

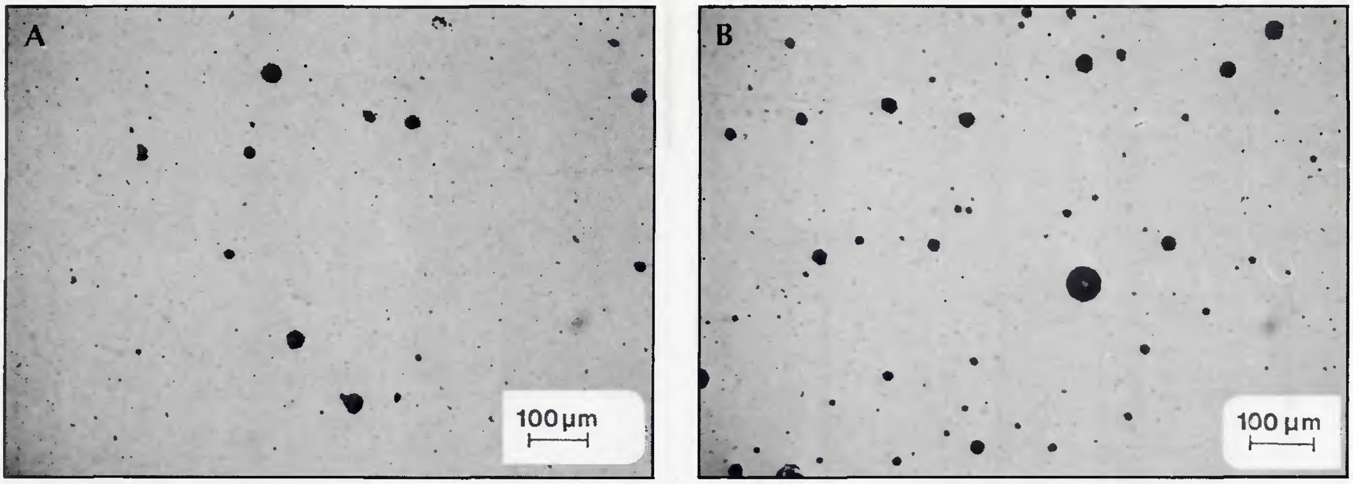

Fig. 5 — Porosity levels in GTA welds from Heat 2 (as-polished). A — Weld made in the environmental chamber; B — weld made outside the chamber.

1 — Fig. 4.

Many of the gas tungsten arc welds on Heat No. 2 made in the environmental chamber completed the bend test without significant cracking. The welds, however, showed some cracking and when these cracks were forced open, they exhibited the presence of porosity. However, the extent of porosity in these welds was much smaller than in the GTA welds made outside the chamber — Fig. 5.

The plasma arc welds made on Heats 2 and 3 completed the bend test without any cracking. These results showed that the plasma arc welds were better than the gas tungsten arc welds. However, the plasma arc welds made using argon as the shielding gas exhibited gross porosity and failed in the bend test even before they experienced a 30-deg bend. Figure 6 shows the difference in the porosity levels between Heat 2 welds made using argon and those made with argon-5% hydrogen as the shielding gas.

The gas tungsten arc welds made on Heat No. 4 showed a considerable amount of porosity — Fig. 7. Yet all welds from this heat completed the bend test without any visible cracking at all. Because no gas tungsten arc weld failures were encountered, no plasma arc welding was attempted on this heat.

Although all the Gleeble specimens survived the bend tests without falling apart, several patterns were evident among the heats studied. For example, Heat 1 showed cracking in the specimen subjected to a peak temperature of 975°C (1787° F), while Heats 2 and 3 did not. Even at a peak temperature of 1025°C (1877° F), where according to Fig. 1 liquid metal should have formed in the alloy, cracks were more numerous, deeper and formed earlier during bending in Heat 1 compared to Heat 2. Thus, it is apparent that Heat No. 1 showed more sensitivity to cracking than Heat No. 2.

Gas Analysis

The results of the gas analyses are shown in Table 3. It can be seen that the level of oxygen remained virtually the same among the various conditions of the samples tested. The nitrogen level in all the samples analyzed was less than 1 ppm and hence considered insignificant. However, the weld metal showed a small pick up of hydrogen compared to the as-homogenized base metal.

The Scanning Electron Microscope Study

The scanning electron microscope examination of the broken welds from Heat 1 showed the presence of several small

Table 3—Gas Analysis Results on Heat 1

Condition of the Samples	Gas Content (ppm) Oxygen(a)	Nitrogen(a)	Hydrogen(b)
As-cast	6	<1	0.14
Homogenized	7	<1	0.18
GTA weld	7	<1	0.54

(a) Average of 5 readings.
(b)Represents sum of the hydrogen liberated through a 25-min 600°C treatment and additional tin-fusion method.

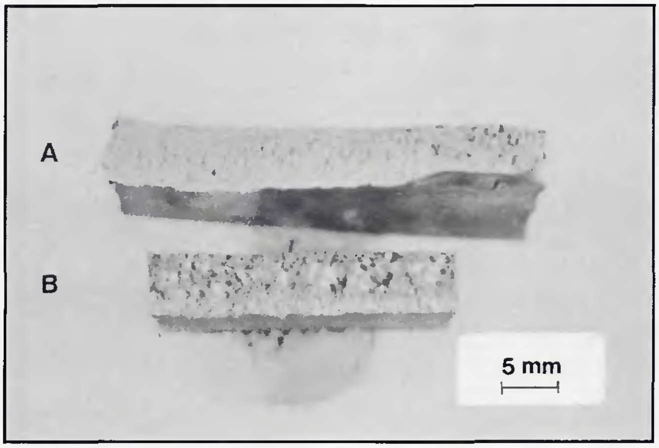

Fig. 6 — Effect of shielding gases on the porosity levels seen in the plasma arc welds. A — Argon + 5% hydrogen; B — argon.

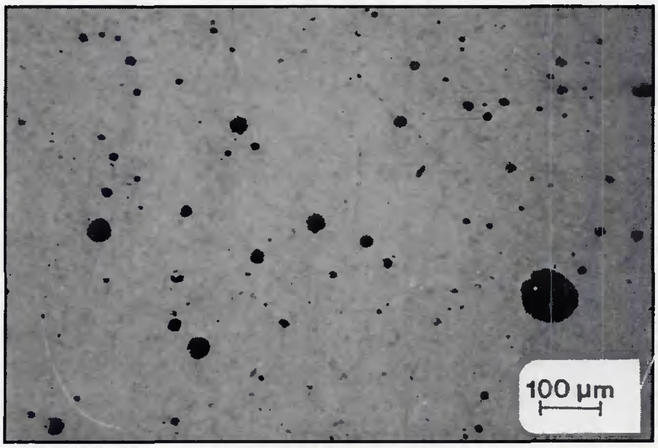

Fig. 7 — Porosity in the GTA welds made on Heat 4 (as-polished).

Fig. 8 — SEM view of the partially melted zone of a weld from Heat 1. Arrows show the cracks found along the grain boundaries. Etched in ferric chloride solution.

Fig. 9 — SEM view of a crack tip (shown by arrow) following Gamma phase (shown by arrowheads).

hairline cracks along the grain boundaries in the partially melted zone — Fig. 8. The cracks were following a grayish-looking phase that formed along the grain boundaries — Fig. 9. This grayish-looking phase was identified with energy-dispersive x-ray (EDX) analysis to be Gamma (γ) with a tin-rich composition. The measured tin content of Gamma phase was often as high as 35 wt-%. The extent of Gamma phase along the grain boundaries was much more prevalent in welds from Heat No. 1. than in the other two heats. A large amount of Gamma phase was found within the grains in Heats 2 and 3.

The SEM examination further revealed that the fine cracks seen in the partially melted zone exhibited interdendritic morphology — Fig. 10. This suggests that the cracks were following the interdendritic areas in the liquated regions of the partially melted zone. At several locations, large networks of Gamma were found covering many of the pores — Fig. 11. A similar interdendritic morphology was observed in the cracks from the Gleeble specimens.

Some of the pores in the welds from Heat Nos. 2 and 3 showed the presence of a deposit at the bottom of the pits — Fig. 12. The EDX analysis indicated that these deposits were rich in manganese and phosphorus.

Optical Metallography

Optical metallographic observations confirmed that the cracks in specimens from Heat No. 1 were initiating and propagating along the Gamma phase that formed in the interdendritic regions — Fig. 13. The many large pores seen in many of the samples were surrounded by a network of Gamma phase — Fig. 14. Although porosity was observed in the welds from Heat No. 4, no cracking was evident either in the as-welded specimens or the bend-tested specimens.

The study of the Gleeble specimens revealed that the size and the extent of porosity were worse in Heat No. 1 than in Heat Nos. 2 and 3. The extent of Gamma formation was clearly noticeable in specimens from Heat No. 1 even at a test temperature of 950°C, whereas the other two heats showed the presence of Gamma only after a peak temperature of 975°C was reached. Again, Heat No. 1 showed the presence of Gamma along the grain boundaries, sometimes in networks, leading to crack formation. Figure 15 shows the presence of cracking along the grain boundaries in a specimen from Heat No. 2 that was subjected to a peak temperature of 1000°C (1832°F). The presence of grayish-looking Gamma phase can also be noted along the grain boundaries. However, both Heat Nos. 2 and 3 showed a considerable amount of Gamma phase within the grains. In general, all three heats showed the presence of more Gamma in the specimens as the peak temperature to which they were subjected to was raised; this suggests that grain-boundary melting increased in the specimens as the peak temperature was increased. In addition, all the specimens exhibited spherical porosity indicative of gas evolution.

Discussion

The results clearly showed that the cause of weld failures in the bend tests for specimens from Heat No. 1 was the formation of brittle intermetallic phase Gamma along the grain boundaries in the partially melted zone. The formation of large pores in the weld also caused some weld cracking but the actual failures occurred in the partially melted zone. Evidence was found to indicate that crack initiation and propagation, at least in the initial stages, occurred preferentially along the Gamma phase regions. The interdendritic morphology seen in the cracks in the partially melted zone of both the weld and the Gleeble specimens shows that the Gamma regions were molten during welding and resolidified during the cool-down

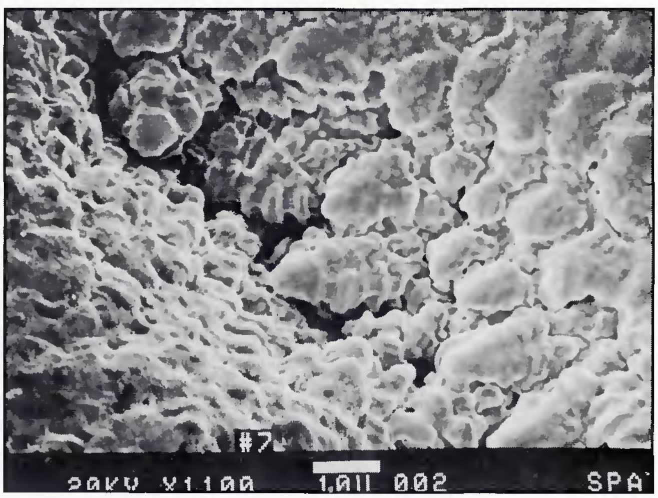

Fig. 10 — SEM view of a crack surface showing interdendritic morphology.

Fig. 11—A—SEM view showing a pore covered with a network of Gamma phase; B—higher magnification view of Gamma regions.

cycle. When formed in clusters, cracks can easily initiate in the brittle Gamma phase; these cracks can propagate later during bending of the weld and Gleeble specimens.

Manganese and phosphorus are added to copper alloys for deoxidation purposes. During welding, the weld metal in Heats 2 and 3 also exhibited better fluidity compared to the welds from Heat 1. It is believed that the addition of manganese and phosphorus may have been responsible for this change. The fact that more Gamma was found within the grains in Heats 2 and 3 suggests that manganese- and phosphorus-rich precipitates may have nucleated the formation of Gamma within the grains. Gamma formation was noticed in Gleeble specimens from Heats 2 and 3 only after a peak temperature of 975°C was reached. This indicates that the addition of manganese and phosphorus to the melts raised the solidus temperature of the alloy.

The fact that many of the large pores in the weld were surrounded by large networks of Gamma (Fig. 14) may mean that the gases responsible for porosity may have evolved from the Gamma phase. This is entirely possible because as solidification proceeds, the last liquid to solidify is enriched in gases such as hydrogen and oxygen (Ref. 8). These two gases can result in the formation of hydrogen and steam, which together cause large pores to occur in the weld. Because the amount of nitrogen in the weld metal, as well as in the base metal prior to welding, is less than 1 ppm, it is unlikely that nitrogen caused the many large pores seen in the weld. The observation that manganese and phosphorus compounds were seen at the bottom of many of the pores may also support the hypothesis that the deoxidation products of these two elements nucleated the formation of Gamma phase within the grains in Heats 2 and 3. The Gamma phase is the last liquid to solidify in the alloy and hence, becomes enriched in hydrogen and oxygen.

Porosity alone did not cause weld failures in the bend tests because welds from Heat No. 4 that showed considerable amounts of porosity survived the bend test without any cracking. Heat No. 4 did not contain tin, and therefore the tin-rich Gamma phase was absent in this heat. This explains why, in spite of the presence of porosity, the welds from this heat survived the bend test. However, when large pores were present, deep cracks were noted in the welds from Heat No. 2 after the bend tests. Therefore, control of porosity is an important step in getting ductile welds. At the same time, reducing the porosity in the welds alone did not produce ductile welds as evidenced by the failure of the plasma arc welds made on Heat 1 using argon - 5% hydrogen as the shielding gas. These plasma arc welds, that showed very little porosity, failed in the bend tests as result of crack initiation at Gamma phase regions. Therefore, it is clear that apart from controlling the porosity in the welds, the formation of Gamma phase along the grain boundaries should also be avoided to improve the ductility of the welds.

The presence of visible porosity in the welds made in the environmental chamber and the Gleeble specimens shows that the source of porosity is dissolved gases in the base material. Although the extent of porosity is reduced with the use of the environmental chamber, in view of the cracking noticed in these welds, the use of such a chamber is not a total solution to the problem. Besides, the use of an environmental chamber is not a feasible solution to weld coils in a production environment.

Kobayashi, *et al.* (Ref. 21), investigated the use of argon-hydrogen gas mixtures for shielding gas in the gas metal arc welding of copper. He found porosity in the welds, which he attributed to the hydrogen in the shielding gas. The present results are in contrast to those of Kobayashi, *et al.* Diatomic gases dissociate in the arc, and recombine at the surface of the workpiece releasing heat (Refs. 7, 29). Therefore, when diatomic gases are

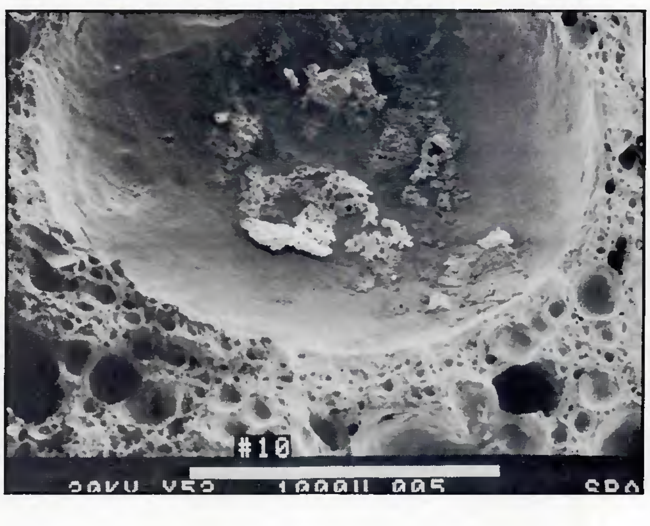

Fig. 12—SEM view of a large pore in a weld from Heat 2 showing deposit at the bottom.

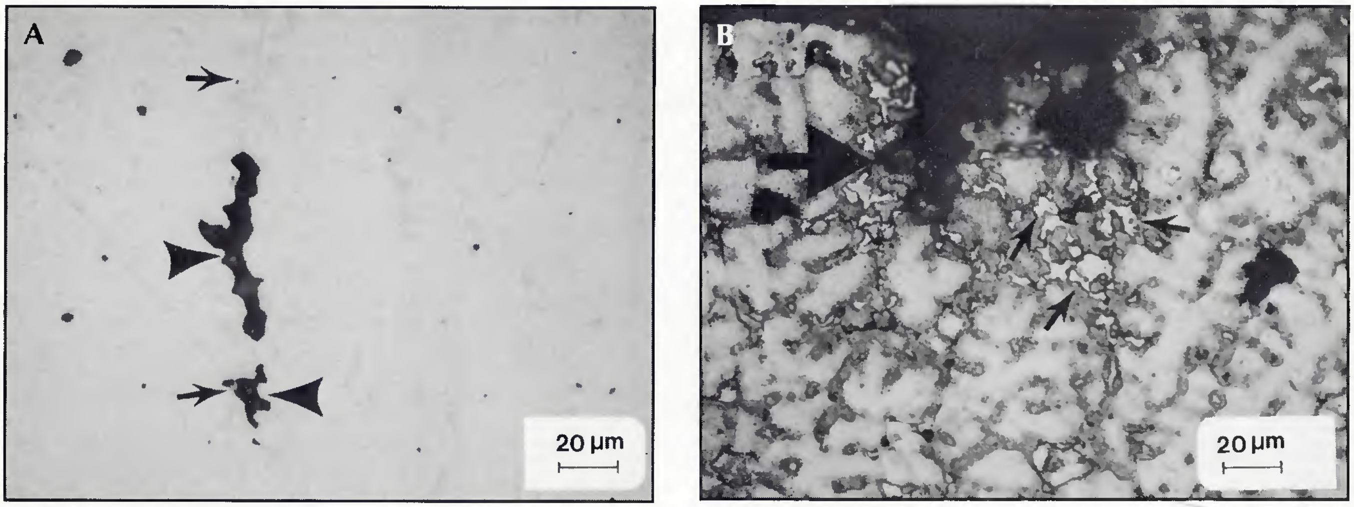

Fig. 13 — A — Cracks (shown by arrowheads) in the partially melted zone of a weld from Heat 1 initiating and propagating along the Gamma phase (shown by arrows) (as-polished); B — crack (shown by large arrow) propagating along Gamma phase (shown by small arrow). Notice the presence of Gamma in interdendritic regions. Etched in ferric chloride solution.

Fig. 14 — Large pores in a weld from Heat 1 surrounded by a network of Gamma phase (shown by arrowheads) (as-polished).

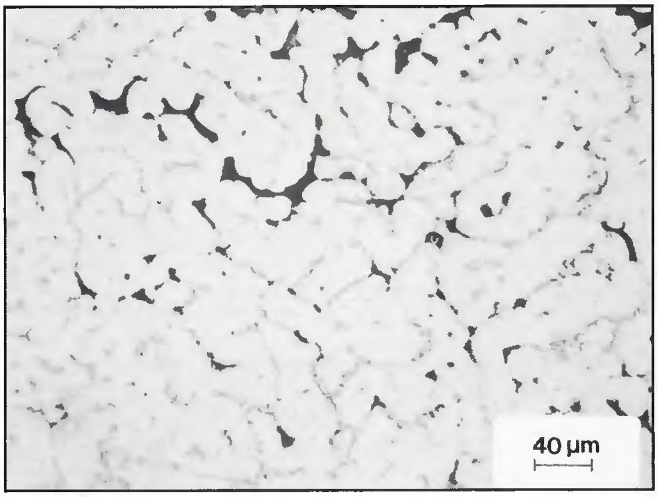

Fig. 15 — Cross-section of a Gleeble specimen from Heat 2 showing the cracks along the Gamma (grayish-looking) phase (as-polished).

present, there is an increase in the anode temperature. Argon-hydrogen mixtures enhance weld-pool wettability, and thus promote uniform weld bead geometry (Ref. 30). Argon-hydrogen mixtures are recommended for applications where porosity is a problem (Ref. 30). The higher arc temperature from the presence of hydrogen also permits the use of faster welding speeds, which in turn, helped reduce the extent of porosity in the welds. The faster welding speed used in plasma arc welding made the porosity finer and more dispersed than in the gas tungsten arc welds. In GTA welding, the slower welding speed allowed more time for the gas bubbles to grow, which resulted in large pores in the weld. The keyhole mode arc in the plasma arc welding caused less melting of the base metals and gave a steeper temperature gradient, all of which resulted in a smaller partially melted zone than in the GTA welds.

Conclusions

Based on the weld ductility study on Cu-9 Ni-6 Sn alloy, the following conclusions may be drawn:

1) The cause of weld failures in the bend tests was the formation of the tin-rich Gamma phase along the grain boundaries in the partially melted zone. Evidence was found to indicate that cracks initiated and propagated along these Gamma regions.

2) Porosity alone was not sufficient to cause weld failures in the bend tests. However, the presence of gross porosity in the weld caused deep cracks to occur that would make the welds unacceptable for service performance.

3) The addition of manganese and phosphorus eliminated the weld cracking that resulted from the Gamma formation at grain boundaries. The heats that contained manganese and phosphorus showed more Gamma within the grains. The addition of zinc did not have any noticeable effect on the weld ductility of the alloy.

4) The use of argon - 5% hydrogen as the shielding gas in plasma arc welding reduced weld porosity noticeably compared to the use of straight argon as the shielding gas. The use of plasma arc in keyhole mode resulted in less melting of the base material and gave a narrower heat-affected zone. As a result, this made the partially melted zone narrow.

5) The use of argon - 5% hydrogen as shielding gas for the plasma arc welding technique and the addition of manganese and phosphorus to the alloy produced ductile welds in Cu-9 Ni-6 Sn alloy.

References

1. Plewis, J. T. 1975. High strength Cu-Ni-Sn alloys by thermomechanical processing. *Metal-*

lurgical Transactions A, Vol. 6A, 3:537–544.

2. Louzon, T. J., and David, M. E. 1982. Microstructural and mechanical property correlation for Cu-10 Ni-8 Sn spinodal alloy. *Microstructural Science,* Vol. 10, White, Richardson, McCall (eds.), Elsevier Publishing Co., Inc.

3. Scorey, C. R., Chin, S., White, M. J., and Livak, R. J. 1984. Spinodal Cu-Ni-Sn alloys for electronic applications. *Journal of Metals,* Vol. 36, No. 11, pp. 52–54.

4. Fox, A. 1979. Stress relaxation in bending of copper-nickel-tin alloy strip strengthened by spinodal decomposition, *Journal of Testing and Evaluation,* Vol. 7, No. 5:286–290.

5. Schwartz, L. H., Mahajan, S., and Plewis, J. T. 1974. Spinodal decomposition in a Cu - 9 wt-% Ni - 6 wt-% - Sn alloy. *Acta Metallurgica,* Vol. 22 (5):601–609.

6. Gaffoglio, C. J. 1979. Copper takes a lot of heat. *Welding Design and Fabrication,* Vol. 52, No. 10, pp. 90–100.

7. Subramanian, V. R. 1976. Weldability and welding of copper and some applications in electrical industry. *Indian Welding Journal,* September, Vol. 8, No. 3, pp. 88–97.

8. *Metals Handbook,* Vol. 15, Ninth Edition, 1988. ASM International, Materials Park, Ohio, pp. 82–87.

9. Anik, S., and Doron, L. 1987. Metal physics processes in the welding of copper and copper alloys — basic chemistry and physics of materials. *Schweissen and Schneiden,* Vol. 39, No. 12, pp. 617–623.

10. Rogerson, J. H. 1984. Significance of welds in copper and cupronickel alloy welds. Their relevance to design and quality standards. *Welding Review,* Vol. 3, No. 4 pp. 192–194.

11. Lawman, J. R., and Rogerson, J. H. 1983. The significance of weld defects in copper calorifiers. *Metal Construction,* Vol. 15, No. 10, pp. 626–627.

12. Woods, P. F. 1968. Welding coppers by modern arc techniques. *Metalworking Production,* 112, (16):47–48.

13. Korenyuk Yu, M., Petrov, G. L., and Kalinina, M. I. 1972. Modeling the conditions under which pores are initiated during the welding of copper. *Welding Production,* Vol. 19, No. 5, pp. 1–3.

14. Nazerenko, O. K., Agarkov, V. Ya, Ikonnikov, V. I., and Solyanik, N. Kh. 1987. Effects of the method by which the weld edges are treated on the formation of pores in welds during the electron beam welding of copper. *Welding International,* Vol. 1, No. 1, pp. 6–10.

15. Uda, M., and Ohno, S. 1973. Porosity formation in weld metal. Report I: effect of hydrogen on porosity formation in pure aluminum at non-arc melting. *Journal of the Japan Welding Society,* Vol. 42, No. 3, pp. 225–235.

16. Dzhevaga, I. I. 1968. A study of pore formation during the automatic electric arc welding of copper and its alloys. *Svar. Proizv.,* (9):1–6.

17. Littleton, J., and Jordon, M. F. 1975. Steam porosity formation in tungsten inert gas welding of copper. *Metals Technology,* 2 (6):268–278.

18. Howden, D. G., and Milner, D. R. 1963. Hydrogen absorption in arc melting. *British Welding Journal,* No. 10, pp. 304–316.

19. Littleton, J., Lammas, J., and Jordon, M. F. 1974. Nitrogen porosity in gas shielded arc welding of copper. *Welding Journal* 53(12):561-s to 565-s.

20. Kobayashi, T. 1972. Possibility of argon-nitrogen gas metal arc welding of some nonferrous metals. *Proceedings of the International Conference on Welding and Fabrication of Non-Ferrous Metals,* Abington, Cambridge, England, The Welding Institute, Vol. 1, pp. 17–24.

21. Kobayashi, T., Kuwana, T., Ando, M., and Fujita, I. 1970. The gas metal arc welding of copper. *Transactions of the Japan Welding Society,* Vol. 1, No. 1, pp. 61–71.

22. Kuwana, T., Kokowa, H., and Honda, A. 1987. Effects of nitrogen and titanium on porosity and microstructure in Ar-N_2 gas metal arc welded copper. *Transactions of the Japan Welding Society,* Vol. 18, No. 2, pp. 159–166.

23. Leibzon, V. M., Glushko, V. Ya., Lositskii, N. T., and Artemov, N. S. 1976. A filler wire for the welding of copper in nitrogen. *Welding Production,* Vol. 23, No. 1, pp. 72–73.

24. Sapiro, L. S. 1972. Evolution of ammonia during boiling and recrystalization of the metal of a weld pool. *Welding Production,* Vol. 19, No. 7, pp. 7–10.

25. Sheer, B. Sh., and Asnovskaya, G. A. 1976. An examination of the composition of the gas in pores in brazed joints. *Welding Production,* Vol. 19, No. 7, pp. 7–10.

26. Brandon E. 1969. Weldability of oxygen-free, boron-deoxidized and deoxidized low-phosphorus copper. *Welding Journal* 48(5):187-s to 193-s.

27. ASTM Standard: B 740-87. 1988. Standard specification for copper-nickel-tin spinodal alloy strip. ASTM, Philadelphia, Pa.

28. *Welding Handbook,* Vol. 2, Seventh Edition. Ed. W. H. Kearns. 1978. American Welding Society, Miami, Fla., pp. 301–303.

29. Howden, D. G. 1969. Mass transfer of metal vapor and anode temperatures in arc melting. *Welding Journal* 48(3):125-s to 132-s.

30. *Metals Handbook,* Vol. 6, Ninth Edition, 1988. ASM International, Materials Park, Ohio, pp. 198–199.